Escola de Primavera de Transição e Turbulência
Blumenau 2022

13th Spring School on Transition and Turbulence
September 19th-23rd, 2022, Blumenau, SC, Brazil

EPTT-2022-0058
Experimental and Numerical Characterization of an Isothermal Natural Gas Jet in the Near Field of an Open Mini Gas Injector

William A. C. Ibañez
Western Paraná State University, Foz do Iguaçu - PR, Brazil
william.ibanez@unioeste.br

Márcio J. E. Demétrio
Amir A. M. de Oliveira Jr.
Federal University of Santa Catarina, Florianopolis - SC, Brazil
marcio.demetrio@gmail.com , amir.oliveira@gmail.com

Fernando Marcelo Pereira
Federal University of Rio Grande do Sul, Porto Alegre - RS, Brazil
fernando.pereira@ufrgs.br

Abstract. *The radial and axial velocity and turbulence intensity profiles were measured using the hot-wire technique and predicted by numerical simulation in the near field at the outlet of three mini gas injectors used in atmospheric burners. The gas injectors have 1.5 mm of orifice diameter and a cup-like region at the outlet. The working fluid is natural gas and the orifice Reynolds number was fixed at 3060 for all measurements. The radial velocity profiles were measured at a distance of 0.48 mm from the injectors outlet and their characteristics determine the development of the jet shear layer. While injector 1 provides an initially laminar shear layer, injector 3 results in an unstable shear layer, with the presence of high velocity fluctuations. These results are confirmed by both the Schlieren measurements and the spectral analysis. The numerical simulations used the γ-Re_θ RANS transition model available in the STAR-CCM+ commercial package. The numerical results provide a jet spreading rate slightly bigger than the measurements suggest for injector 1 and an overall behavior well predicted for injector 3. Injector 2 presented larger deviations, since the effect of the internal mixing layer in the cup region was not well predicted numerically.*

Keywords: *Gas injectors, transition flow, hot-wire anemometry, atmospheric burners*

1. INTRODUCTION

Gas burners for domestic cooking ranges and ovens operate with a sub stoichiometric gas-air mixture, i.e., the amount of oxygen in the mixture at the burner orifices is smaller than the amount needed to provide complete combustion to saturated products. The primary fuel-air mixture is formed when a jet of fuel gas is directed to the entrance of a venturi pipe. The transfer of linear momentum from the jet to the ambient air promotes air entrainment and mixing. The pressure drop downstream from the venturi entrance is determined by the geometry and power of the burner. The gas fuel is fed at constant pressure, regardless of the burner power. Therefore, the amount of air entrainment for a given venturi pipe and burner is determined by the shape of the gas injector. Figure 1 presents photographs of flames obtained in a table-top burner operating with G20 fuel gas fed at the pressure of 2 kPa (gauge), burner power of 2.2 kW (based on HHV), using the three different injectors, with the same injector orifice diameter of 1.5 mm and same distance from the inlet of the venturi in respect to the outlet of the injector. The Brazilian Standard NBR 13723-1 (ABNT, 2004) defines the basic properties of the G20, G30 and G31 family of reference fuel gases for domestic cooking. G20 is representative of natural gas while G30 and G31 are representative of the LPG fuels. In the figure, the injectors 1 and 2 provide acceptable flames for this application, injector 3 results in a excessively rich flame which produces soot wings. The reason for the low primary air for injector 3 is the cup shape of the exit region, which decreases the momentum transfer from the free jet to the ambient air, thus decreasing the amount of air entrainment. In the applications in domestic and commercial cooking systems, the gas pressure is usually fixed. The appliance and burner design define the power and available space for installing the gas injecting system.

A large number of studies were developed for axisymmetric jet flows emerging from tubes and smooth contraction nozzles and they produced an overall solid understanding of these flows. The jet is divided in three characteristic regions: an initial near field region downstream the exit, a transition region, and a self-preserving far field region further downstream. The majority of the studies for jet flows focused the far field of fully turbulent jets, with orifice Reynolds numbers above 10,000. These studies set the basis for the similarity conditions that apply in the far field. The effects of the internal

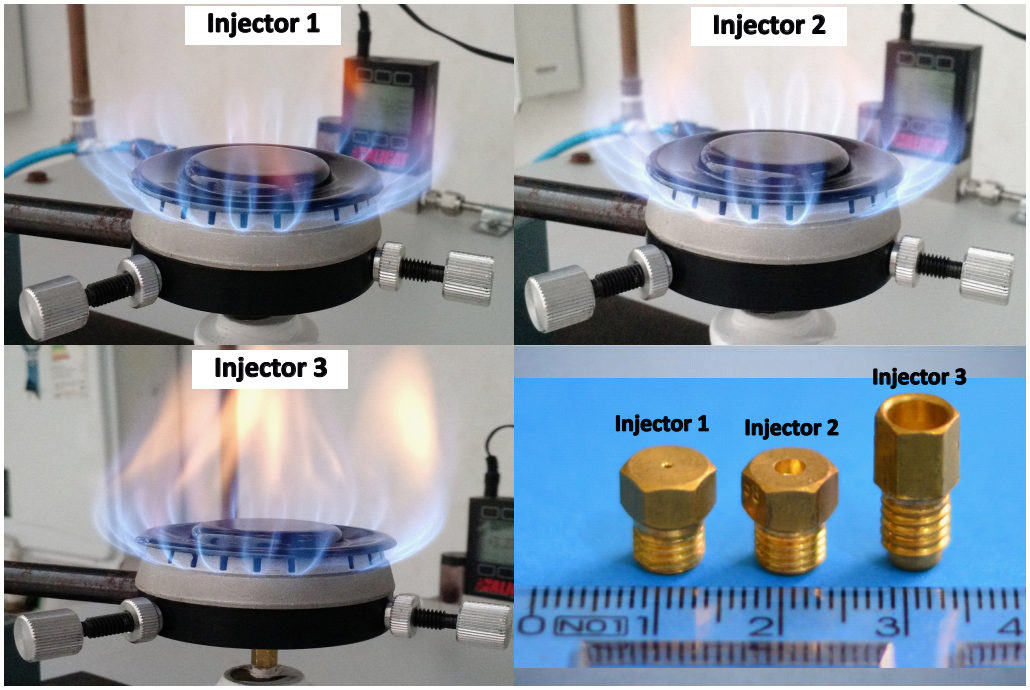

Figure 1. Photographs of flames obtained in a table-top burner operating with natural gas fed at the pressure of 2 kPa (gauge), burner power of 2.2 kW (based on HHV), using the three different injectors, with the same injector orifice of 1.5 mm.

flow and boundary conditions in and around the orifice exit develop along the zone of flow establishment (ZFE), which includes the near and the transition regions. This zone corresponds to a so called preserving core region (Vouros and Panidis, 2013), where characteristics of the initial velocity profile determine the development of the shear layer. A parameter commonly utilized to describes the initial nature of the boundary layer is the shape factor H_{12} according to Schlichting (1979). This parameter is calculated by the relation between the displacement thickness δ_1 and momentum thickness δ_2 defined as

$$\delta_1 = \int_0^{D/2} \left(1 - \frac{\bar{u}(y)}{\bar{u}_o}\right) dy \tag{1}$$

$$\delta_2 = \int_0^{D/2} \frac{\bar{u}(y)}{\bar{u}_o} \left(1 - \frac{\bar{u}(y)}{\bar{u}_o}\right) dy \tag{2}$$

where $\bar{u}(y)$ is the radial profile of the axial velocity component, $\bar{u}_o$ is the average velocity of the jet centerline and $D/2$ is the orifice radius. The shape factors for a laminar and turbulent boundary layer are $H_{12} = 2.6$ and 1.4, respectively (Schlichting, 1979).

In the application in atmospheric burners, the behavior in the near field is key to determine the air entrainment in the fuel jet. The injectors studied here, shown in figure 1, have a complex internal geometry, presenting a conical contraction, a straight orifice, followed by a sudden expansion before reaching the ambient, as well as a relatively thick wall. These details may cause a complete departure from previous findings for straight pipes (Papadopoulos and Pitts, 1998) and contraction nozzles (Kwon and Seo, 2005). There is no study available on the effects of these nozzle details in the jet flow. Therefore, there is still a need to assess the effects of the injector geometry on the mass, momentum, and energy flow for the Reynolds numbers of interest in the applications. For this, the flow in the three injectors of figure 1 is analyzed experimentally and numerically.

2. EXPERIMENT

2.1 Apparatus for Velocity Measurements in the Jet Flow

Figure 2 presents a schematics of the experimental set-up for velocity measurements in the jet flow region using hot wire anemometry. It is mainly composed by the (1) injector, (2) pressure tap, (3) feeding tube, (4) mass flow meter and controller, (5) compressed freon dehumidifier, (6) pressure regulator and filter, (7) micromanometer, (8) three-axis stage, (9) hot-wire probe, (10) support and cable, (11) Mini CTA, 12 VDC power source and connecting box, and (12) a computer for the data acquisition.

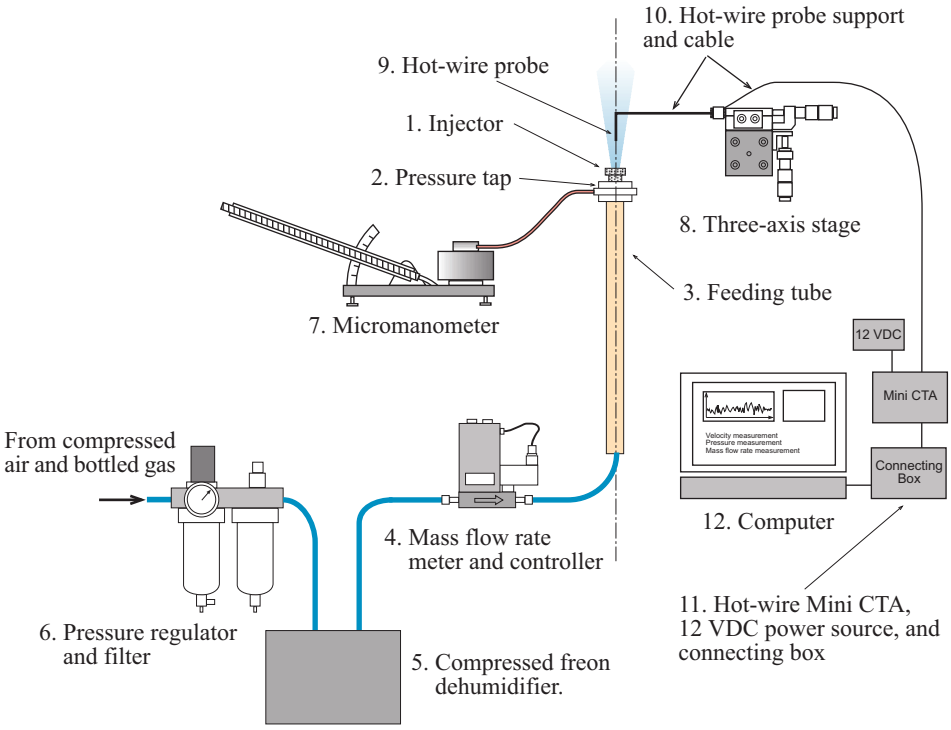

Figure 2. Schematic representation of the experimental set-up for velocity measurements.

The feeding tube is made of brass, it has an internal diameter (D_o) of 8 mm, total length of 300 mm and allows for simple replacement of the injector. At the entrance of the feeding tube is connected an aluminum tube with length 1 m and internal diameter 8 mm such that the total length for fully developing the laminar flow before the injector is 1300 mm ($L/D_o = 162$).

In this work, three injectors were selected. Its geometries are characterized for an external envelope cup-like of different shapes observed for a large number of injectors available to the appliances industry. Figure 4 presents a schematic drawing of the internal geometry of this injectors and the Tab. 1 its main characteristic dimensions. The interior flow path is formed by 5 regions, whose lengths are labeled L_1 to L_5. The diameter of the orifice is $D_2 = 1.5$ mm and is the same for the three injectors. The thickness of the wall at the injector outlet is $e = 6$ mm for injectors 1 and 2 and $e = 2$ mm for injector 3.

Table 1. Characteristic dimensions of the three injectors. The orifice diameter $D_2 = 1.5$ mm is the same for all injectors.

	Dimensions, mm									Angle, deg.	
Injector	D_1	D_2	D_3	L_1	L_2	L_3	L_4	L_5	e	θ_1	θ_2
1	3.5	1.5	–	4.3	3.16	1.54	–	–	3.25	40	–
2	3.0	1.5	2.4	2.83	0.53	2.06	–	3.59	2.8	120	–
3	3.0	1.5	5.0	3.7	0.54	2.62	1.14	6.0	1.0	120	118

The velocity field was measured at the outlet injectors with a single axis, constant-temperature, hot-wire anemometer, Mini CTA model 54T30, from Dantec Inc., with the straight 90 degrees probe model 55P14. The probe has a platinum wire with diameter 5 μm and length 1.5 mm as sensing element and a ceramic body. The measurement system also has a 12 V power source, a controller unit and a USB cable for connection to a computer. The velocity measurements were performed at the rate of 100 kHz with 10^6 samples per measurement point. Natural gas (NG) was used as working fluid from a commercial bottled. The molar composition for the NG obtained by gas chromatography revealed: 0.892 of CH_4, 0.059 of C_2H_6, 0.0181 of C_3H_8, 0.0097 of C_4H_10, 0.015 of CO_2, and 0.0071 of balance N_2.

Mass flow rate was measured and controlled using a thermal mass flow rate controller from Alicat Scientific Inc.. Controller model MC-5SLPM-D, with range from 0 to 5 SLPM, was used in the experiments with the injectors. It presented sensitivity of 0.01 SLPM and estimated uncertainty of ± 0.05 SLPM. Besides, the mass flow rate meter and controller for the natural gas provided a temperature measurement with uncertainty of ± 0.5 ^{o}C. Pressure was measured with an inclined tube precision micromanometer from Lambrecht meteo GmbH with uncertainty of $\pm$ 0.65 Pa.

The measurement procedure for the velocity measurements started with the calibration of the hot-wire anemometer with air flow as recommended by the manufacturer (Jorgensen (2002)). Three nozzles were used for the calibration (with

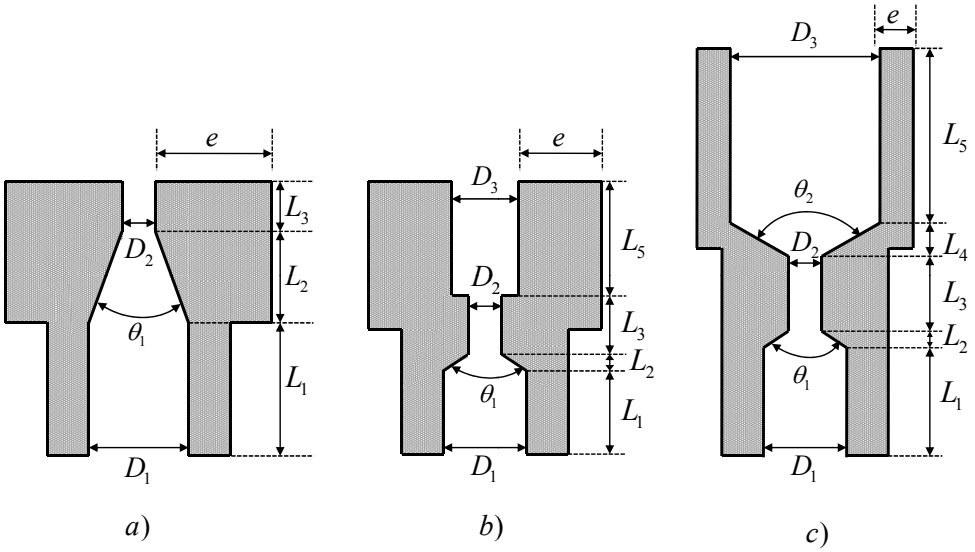

Figure 3. Schematic drawing of the internal geometry of the three injectors (a) Injector 1, (b) Injector 2, and (c) Injector 3.

exit areas of 120 mm^2, 60 mm^2 and 20 mm^2), using dry air and covering the range of velocity from 0.5 to 100 m/s. A fourth degree polynomial was used to curve-fit the voltage versus velocity measurements. The curve fitted predicts the measurements with a confidence interval (for 95 % coverage and $n-5$ degrees of freedom) of $\pm$ 2.8 %. The calibration for natural gas was obtained by converting the data measured with air to natural gas using heat transfer correlations applicable to the CTA, following the recommendations of Pitts and McCaffrey (1985). The natural gas is treated as a pure fluid with the transport properties calculated from Kee *et al.* (1985). During the measurements, great care was taken in identifying the position of the centerline. This was done by moving the probe radially in two directions and detecting the point where the maximum velocity value occurred. The movement of the probe in the x, y and z directions in respect to the injector outlet was performed using a three-axis micrometric positioning table with a precision of $\pm$ 10 μm. The propagated uncertainty of the velocity measurements was estimated as $\pm$ 8 %, following the error propagation analysis described by Moffat (1988).

The Reynolds number for the measurements of the axial velocity was fixed at Re $= 3060$. The radial velocity profiles were measured at a distance of 0.48, 1.2, 3, 6, 8.4, 12, 18, 24 mm from the injector outlet, which corresponds to $z/D_2 = 0.32, 0.8, 2, 4, 5.6, 8, 12$ and 16 respectively. In this work, the profiles measured from $z/D_2 = 0.32$ to 5.6, which corresponds at the near field region of the jet will be presented and discussed. From the measured instantaneous axial velocity u, the average velocity $\bar{u}$ and fluctuation u' are calculated. The relative turbulent intensity is defined as $T_u = \langle\sqrt{\overline{u'^2}}\rangle/\bar{u}$.

After measuring the radial velocity profiles, a mathematical function was curve fitted to the measurements and the moments of the axial velocity were determined from integration assuming axial symmetry. Further data treatment will be presented and discussed in the results section assuming axial symmetry. The data treatment will be presented and discussed in the results section.

2.2 Apparatus for Jet Flow Visualization

Figure 4 presents a schematics of the Schlieren optical technique used to visualize the flow structures in the free jet region at the exit of three injectors. Schlieren optics provide an informative, non-intrusive method for studying transparent and optical media (Settles, 2001).

The system is composed by two oppositely-tilted, on-axis mirrors, a lamp that provide a punctual divergent light source positioned in the focal point of the parabolic mirror 1. Since the light source is at the focal point, the divergent light rays emitted are reflected as parallel rays by the mirror. The mirror 1 is tilted by an angle θ_1, allowing that the light rays collide parallely with a second parabolic mirror, also tilted by an angle θ_2. Consequently, the parallel light rays converge and a knife-edge is positioned in the focal point of the parabolic mirror. The image is recorded in a camera that is positioned behind the knife-edge.

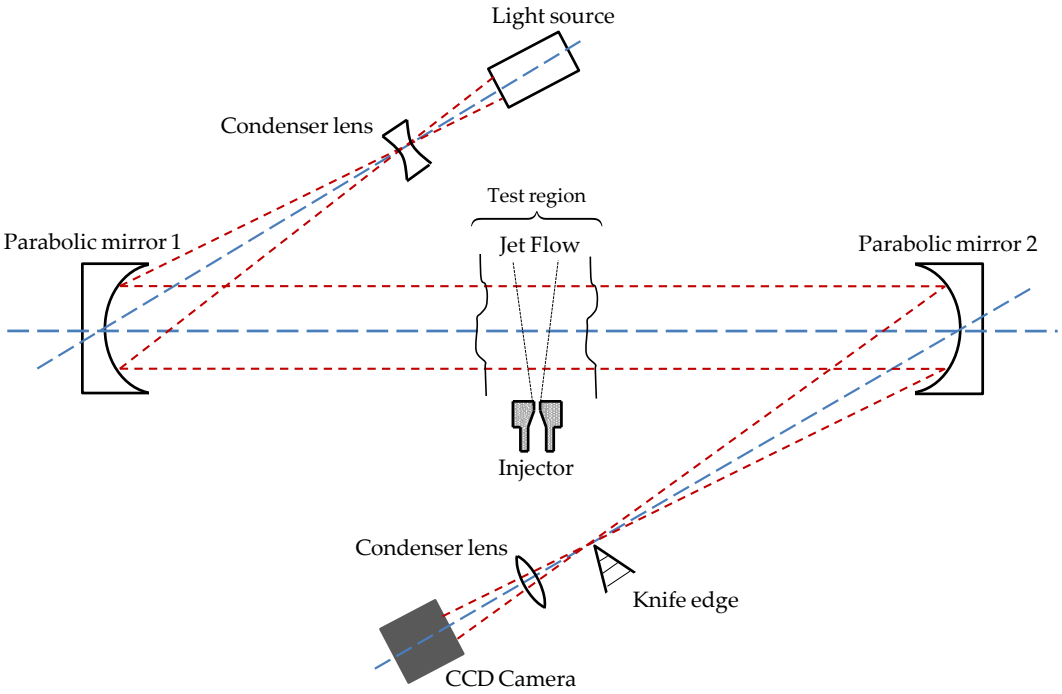

Figure 4. Schematic representation of a Z-type Schlieren arrangement for jet flow visualization.

3. NUMERICAL SIMULATION

Figure 5 presents a sketch of the computational domain used in the numerical simulation of the flow. The problem is modeled as a two-dimensional axisymmetric jet issuing into a quiescent air, where the coordinate axis r, and z denote the radial and axial directions, respectively. The feeding tube has inner diameter $D_o = 8$ mm and length $L_o = 5.6D_o$. This entrance length was deemed sufficient to account for upstream flow development prior to the injector entrance. The injector orifice has diameter $D_2 = 1.5$ mm, as reported in Table 1. The jet develops downstream in a quiescent ambient with length $83D_2$ and width $45D_2$. All simulations were performed with a constant burner power, based on high heating value (HHV), of 2195 W. For this power, the orifice Reynolds number based on the orifice diameter calculated for natural gas is Re = 3060.

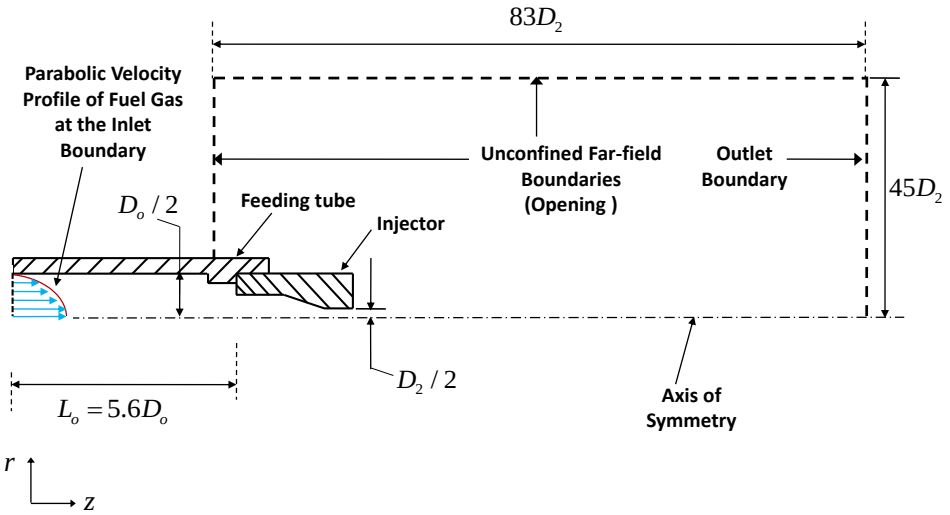

Figure 5. Sketch of the two-dimensional axisymmetric computational domain for injector 1.

The fluids are assumed Newtonian and the flow is steady-state, incompressible and isothermal at 25 °C. The finite volumes commercial code STAR-CCM+® was used to solve the Reynolds-Averaged Navier-Stokes (RANS) model. In

order to predict all flow regimes of a free round jet, the four equations $\gamma - \mathrm{Re}_\theta$ SST transition model was used for turbulence closure. The governing equations were solved using the segregated finite volume flow solver. A second-order upwind scheme was selected for computing the convection flux on the cell face. The convergence criteria for all simulations was defined considering a maximum step of 30000 iterations, allowing a drop of 4 to 5 orders of magnitude in the residuals of the momentum, continuity, turbulence and concentration of the O_2 species.

The boundary conditions were set as follows: At the inlet, a laminar velocity profile for fully developed flow was imposed, as well as a low turbulence intensity level at 0.2 %, based on the measurements for the jet flow at the exit of the injector. Besides, the mass fraction of natural gas was $Y_f = 1$. At the walls, the impermeability and no-slip conditions $\mathbf{v} = 0$ were imposed. At the jet centerline, a symmetry condition was applied. At the outlet (the far-field), zero static pressure, opening conditions and the mass fraction of fuel $Y_f = 0$ were also imposed.

The mesh is formed with polyhedral, quadrilateral and prism elements. In order to resolve the boundary layers, 50 layers of prism elements were used in the 0.15 mm layer near the wall. The first prism layer has a thickness of 0.002 mm to ensure that at least one cell is in the viscous sublayer (i.e., $y^+ < 1$). Quadrilateral elements with sizes smaller than 0.01 mm were used in the gas injector and the free jet region up to a distance of 20 D_2 downstream of the injector based on a mesh independence study performed for injector 1. The remained of the computational domain is filled with polyhedral elements with a maximum size of 0.1 mm. Thus, a total cells number of 1.08×10^6, 1.24×10^6, and 1.58×10^6 were obtained for injectors 1, 2 and 3, respectively. The CPU time required to reach convergence of injector meshes was around in 100 hours. The numerical simulations were performed in an Intel® Core™ i5 processor, 16 GB RAM and processor base frequency of 3.33 GHz. The maximum value obtained for y^+ was smaller than 0.1 for all meshes. We notice that the numerical uncertainty due to discretization errors based on Grid Convergence Index method GCI proposed by Roache (1994), Roache (1997) is smaller than 0.015 %.

4. RESULTS AND ANALYSIS

Figure 6 presents a photograph of the turbulent structures for jets issuing from the three different injectors operating with natural gas, the same injector orifice diameter of 1.5 mm and Re=3060. The measurements shown that, injector 1 provides a shear layer with laminar characteristic in the near field of the jet flow while injectors 2 and 3 that presents a cup-like geometry at the exit region, the jet leaves the orifice with a turbulent appearance.

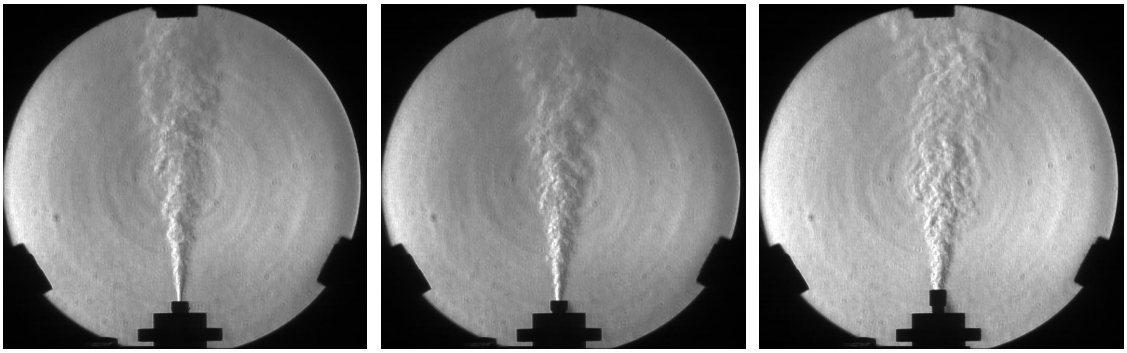

a) **b)** **c)**

Figure 6. Visualization of turbulent structures for the jet flow obtained from Schlieren technique at the exit injectors for Re=3060 and NG. a) Injector 1, b) Injector 2, c) Injector 3.

Figure 7 presents a comparison between the measured and numerical results for axial velocity component at the axial position $z = 0.48$ mm downstream from the injectors outlet section. For injectors 1 and 2, Fig. 7(a) and (b), respectively, the radial coordinate is expressed in terms of the similarity variable η in order to collapse the velocity profiles in the potential core region of the jet. The similarity variable η is defined as,

$$\eta = \frac{(r - r_{0.5})}{\delta_m} \tag{3}$$

where $r_{0.5}$ is the radial coordinate and δ_m is the thickness of the mixing layer defined as,

$$\delta_m = r_{0.9} - r_{0.1} \tag{4}$$

where $r_{0.9}$ and $r_{0.1}$ are the radial coordinates where $u(r, z)$ is 90 % and 10 %, respectively, of the maximum velocity at the jet centerline $u(0, z)$. For injector 3, Fig. 7(c), the radial coordinate is expressed in terms of the similarity variable ξ for fully turbulent jets, defined as

$$\xi = \frac{r}{r_{0.5}}. \tag{5}$$

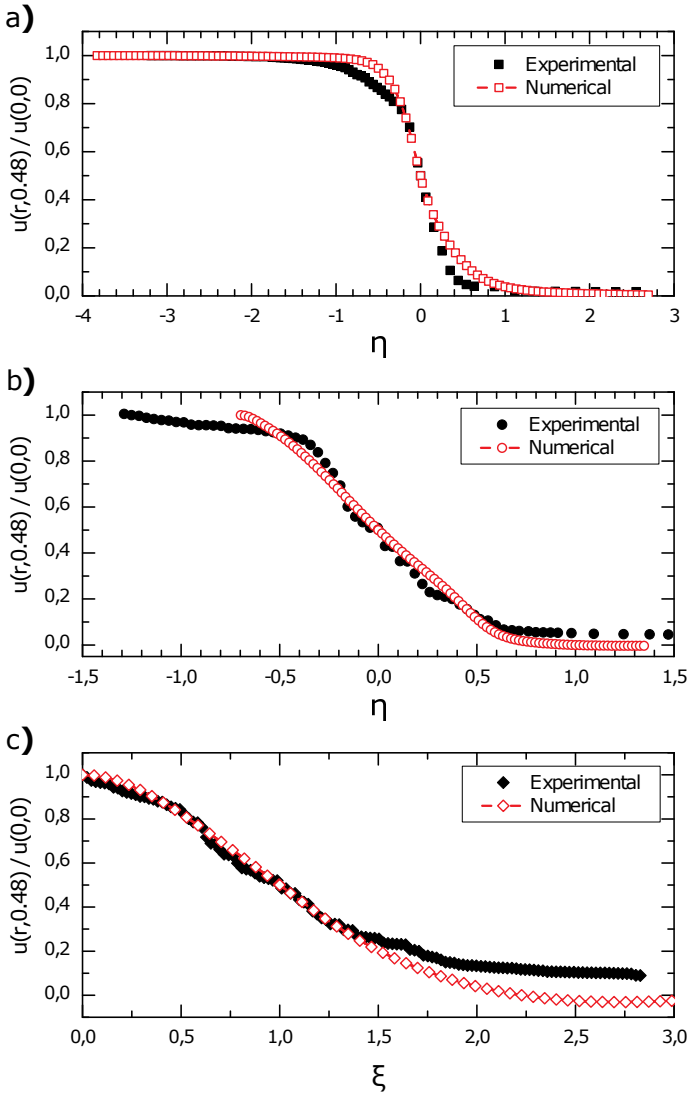

Figure 7. Comparison between the measured and numerically predicted axial velocity component at the axial position $z = 0.48$ mm downstream from the injectors outlet section: a) injector 1, b) injector 2, and c) injector 3. The symbols in the predicted results indicate the position of the nodes of the numerical grid used.

For injector 1, Fig. 7(a), the numerical results predict a slightly more intense spread of the jet into the external ambient than the measurements suggest, but the overall comparison can be considered adequate. For injector 2, Fig. 7(b), the prediction of the jet spread in the external ambient is adequate, but the effect of the internal mixing layer is not well predicted. This indicates a possible deficiency of the numerical model in predicting the flow separation and the turbulence development in the cup region. We notice, also, that the numerical solution predicts slightly negative velocities for $\eta > 0.5$, corresponding to the presence of a reverse air flow in the external ambient near the injector walls, as shown in Fig. 7(b). This reverse flow is not captured by the measurements of the single hot-wire probe used in this work. For injector 3, Fig. 7(c), the overall behavior is well predicted. The numerical solution again predicts slightly negative velocities for $\xi > 1.5$, which is not detected by the measurements of the single hot-wire probe used in this work.

To characterize the initial jet shear layer at the exit region of the three injectors was estimated the shape factor H_{12} following Eq. (1). Thus, the boundary layer integral parameters were obtained integrating numerically the radial profile of the axial velocity component measured at an axial position 0.48 mm ($z/D_2 = 0.32$) downstream from the injectors outlet section. Figure 8 shows a zoom of the velocity profiles at the boundary layer region for the three injectors. For each injector, the local axial velocity u(r,0) and the radial coordinate h were normalized by the maximum velocity u(0,0) and the radius of the outlet section for each injector $R_{s,i}$, respectively, where $i = 1, 2, 3$ are the injectors. Here, h is defined as the distance measured from border up to centerline of the jet. The jet boundary for each injector is obtained based on the radial coordinate $r_{0.5}$, which the local axial velocity u(r,z) is half of the maximum velocity at the jet centerline u(0,z). The profiles shown in Fig. 8 are an indicative of the boundary layer within the injector orifice.

Figure 8a presents the experimental and numerical velocity profiles and compared to the Blasius profile and power law (exponent $n = 5$ and 7) for laminar and turbulent flow, respectively. We notice that the numerical results measured

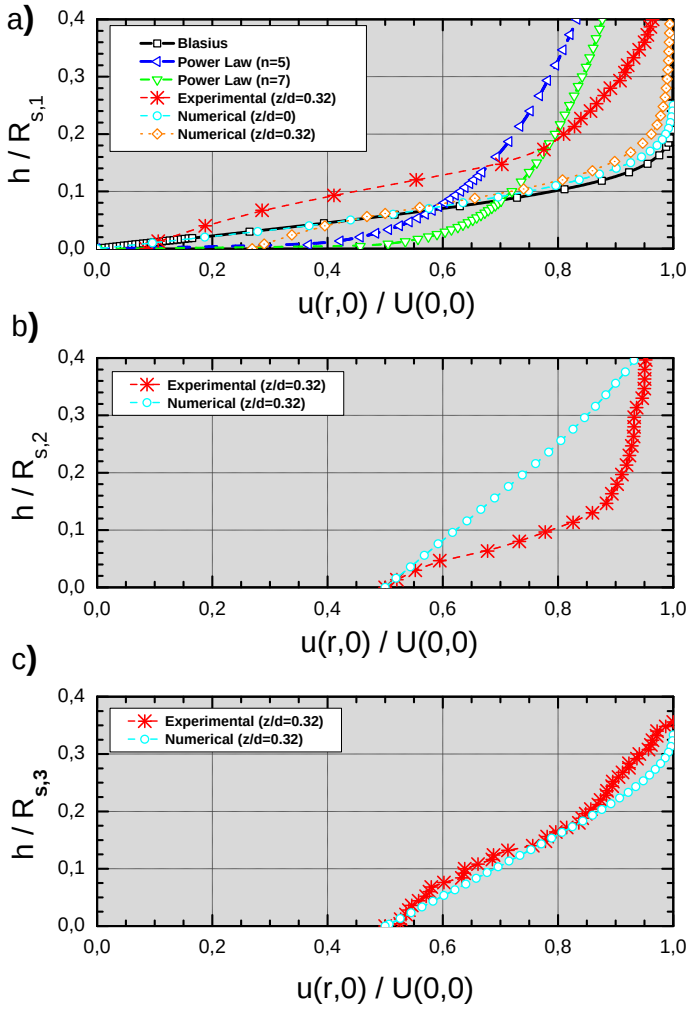

Figure 8. Comparison between the measured and numerically predicted radial velocity profile near to boundary layer region $z = 0.48$ mm downstream from the injectors outlet section: a) injector 1, b) injector 2, and c) injector 3.

both at $z = 0.0D_2$ and $z = 0.32D_2$ describes an initial laminar shear layer for the jet flow at the exit region of the injector 1, with the theoretical shape factor value of $H_{12} = 2.6$ for the Blasius laminar profile as described for Schlichting (1979). However, the measured profile at $z = 0.32D_2$ describes a shear layer in transition to turbulence with shape factor $H_{12} = 1.75$, being that $H_{12} = 1.4$ is for a turbulent shear layer (Schlichting, 1979). These comparisons show a discrepancy of the single hot-wire probe to predict correctly the velocity profile at the injector outlet. For injectors 2 and 3 in Fig. 8b and c respectively, the profiles were not compared with the Blasius and power law once the profiles presented a slight expansion into the cup region from these injectors. The numerical predictions for injector 2 shown a discrepancy in relation to the measured values while for injector 3, the profile is predicted correctly at an axial distance $z = 0.32D_2$ from outlet sections of these injectors. The shape factors for injectors 2 and 3 estimated of the measured values were 1.67 and 1.99 respectively, describing an initial shear layer of the jet flow in transition for turbulence regime. Table 2 presents a summary of shear layer displacement thickness (δ_1), momentum thickness (δ_2) and the shape factors (H_{12}) obtained from measurements for the three injectors.

Table 2. Shape factors, displacement thickness and momentum thickness obtained from measurements at the outlet section for the three injectors.

Injetor	δ_1(mm)	δ_2(mm)	H_{12}
1	0.119	0.068	1.75
2	0.144	0.086	1.67
3	0.394	0.198	1.99

Figure 9 presents the radial profiles of the turbulence intensity T_u measured at the axial position $z = 0.48$ mm downstream from the injectors outlet section. For injector 1, Fig. 9(a), the turbulence intensity profile is uniform in the jet potential core up to a radius $r/R_3 = 0.8$. These relatively low values of T_u of about 2 % throughout the constant-velocity region of the jet section as shown in Fig. 7a indicate that the jet presents a laminar shear layer at the outlet of injector 1.

Injector 2, Fig. 9(b), presents two peaks of turbulence intensity of 7 % and 4.5 % located at $r/R_3 = 0.083$ and $r/R_3 = 0.733$, respectively. The locations of the peaks in turbulence intensity correspond to local maximums of the mean velocity gradient. The first peak of $T_u = 7$ % located near the jet centerline indicates the transition to a turbulent jet. The second peak of $T_u = 4.5$ % located at $r/R_3 = 0.7$ is indicative of turbulence created in the mixing layer with the external ambient. For injector 3, Fig. 9(c), there is a slight first peak at the centerline which is overshadowed by a strong second peak of $T_u = 18$ % at $r/R_3 = 0.3$, in the mixing layer with the external ambient.

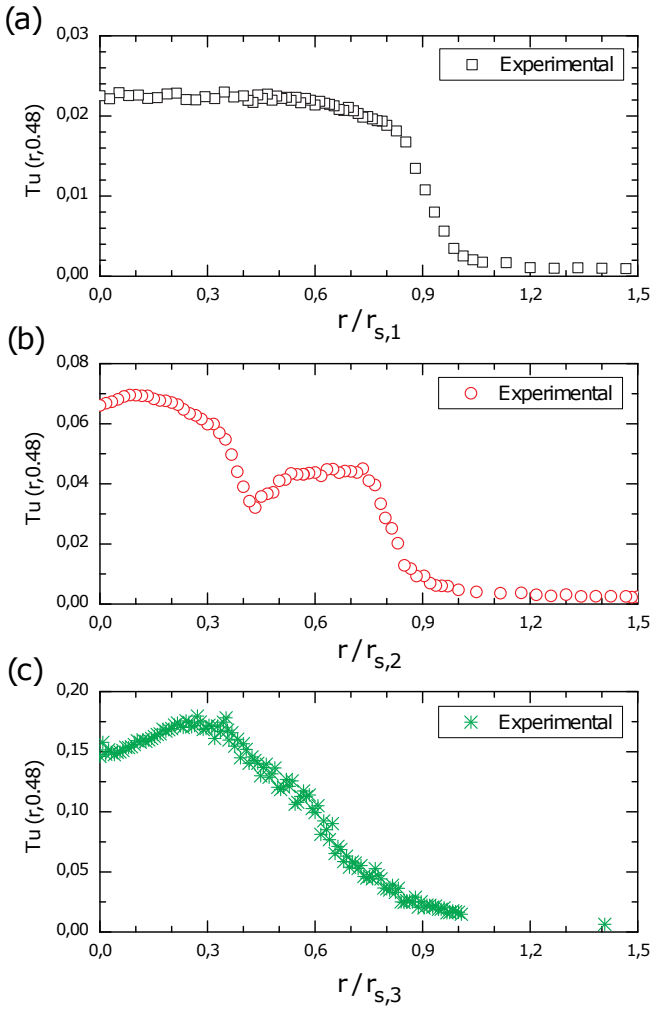

Figure 9. Radial profiles of the turbulence intensity measured at an axial position $z = 0.48$ mm downstream from the injectors outlet section: a) injector 1, b) injector 2, and c) injector 3.

Figure 10 presents the power spectra obtained by applying the Fourier transform (FFT) to the measured instantaneous velocity at an axial distance of $z/D_2 = 0.32$ from outlet section of the three injectors. For injectors 1 and 2, the low energy of spectra confirms an initial laminar shear layer. Injector 3 is characterized for a turbulent shear layer once presented a high energy due to the high turbulence intensities values as show in Fig. 9c. Finally, some sharp high-frequency peaks for sprectrums of injectors 1 and 2 can be attributed to some noise in the signal.

5. CONCLUSIONS

This study analyzed the flow in three different injector geometries commonly used in table-top atmospheric burners for domestic appliances. The measurements included fluid flow rate, the pressure drop along the injector, the axial velocity profile and the turbulent intensity in the outlet of the injectors. Numerical simulations were used to predict the overall flow patterns and to provide supporting information for the analysis of the measurements. The analyses shown an initial laminar shear layer for injector 1 while injector 3 presented a shear layer with turbulent appearance. The numerically

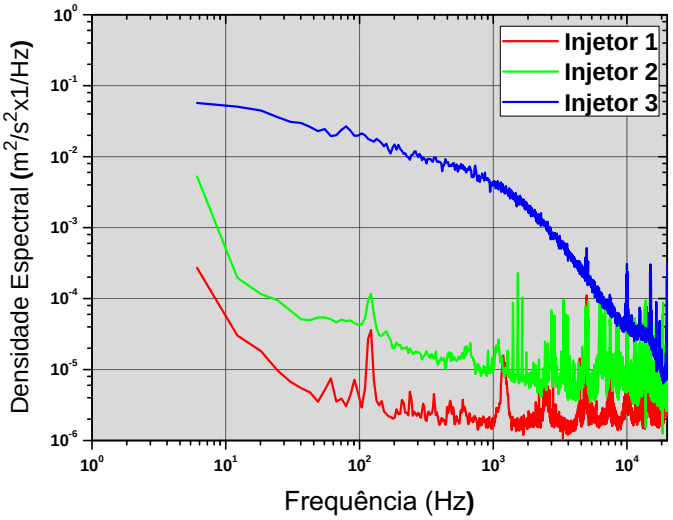

Figure 10. Power spectra of velocity signals measured at an axial distance of $z/D_2 = 0.32$ from jet centerline for the three injectors and $\mathrm{Re}_2 = 3061$.

predicted axial velocity profiles at the outlet of the injectors compared well with the measurements for injectors 1 and 3, but presented deviations for injector 2, possibly meaning a poorer performance of the numerical model. Besides, the numerical solution showed that injectors 2 and 3 present a counter flow near to the wall of the cup region that forms a mixing layer with the out flowing jet.

6. REFERENCES

ABNT, 2004. *NBR13723-1: Domestic cooking appliance burning gas - Part 1: Performance and safety (in Portuguese)*. Brazilian Standard, Brazilian Association of Standards, ABNT, São Paulo, Brazil.

Jorgensen, F.E., 2002. "How to measure turbulence with hot-wire anemometers - a practical guide". Technical report, DANTEC Dynamics, Dantec Dynamics A/S, P.O. Box 121, Tonsbakken 16-18, DK-2740 Skovlunde, Denmark. Publication no.: 9040U6151. Date 2002-02-01.

Kee, R.J., Grcar, J.F., Smooke, M.D. and Miller, J.A., 1985. "A fortran program for modeling steady laminar one-dimensional premized flames". Technical report.

Kwon, S. and Seo, I., 2005. "Reynolds number effects on the behavior of a non-buoyant round jet". *Experiments in Fluids*, Vol. 38, pp. 801–812. doi:10.1007/s00348-005-0976-6.

Moffat, R.J., 1988. "Describing the uncertainties in experimental results". *Exp. Thermal Fluid Sci.*, Vol. 1, No. 1.

Papadopoulos, G. and Pitts, W.M., 1998. "Scaling the near-field centerline mixing behaviour of axisymmetric turbulent jets". *AIAA Journal*, Vol. 36, No. 9.

Pitts, W.M. and McCaffrey, B.J., 1985. "Response behavior of hot wires and films to flows of different gases". Nist interagency/internal report, nbsir 85-3203, National Institute of Standards and Technologies.

Roache, P.J., 1994. "Perspective: A method for uniform reporting of grid refinement studies". *Fluids Engineering*, Vol. 116, pp. 405–413.

Roache, P.J., 1997. "Quantification of uncertainty in computational fluid dynamics". *Annu. Rev. Fluid. Mech.*, Vol. 29, pp. 123–160.

Schlichting, H., 1979. *Boundary Layer Theory*. McGraw-Hill, New York, 7th edition.

Settles, G.S., 2001. *Schlieren and shadowgraph techniques: visualizing phenomena in transparent media*. Springer, Berlin, 1st edition.

Vouros, A. and Panidis, T., 2013. "Turbulent properties of a low reynolds number, axisymmetric, pipe jet". *Experimental Thermal and Fluid Science*, Vol. 44, pp. 42 – 50.

7. RESPONSIBILITY NOTICE

The following text, properly adapted to the number of authors, must be included in the last section of the paper: The author(s) is (are) the only responsible for the printed material included in this paper.